

Enhanced Luminescent Stability through Particle Interactions in Silicon Nanocrystal Aggregates

Joseph B. Miller, Naveen Dandu, Kirill A. Velizhanin, Rebecca J. Anthony, Uwe R. Kortshagen, Daniel M. Kroll, Svetlana Kilina, and Erik K. Hobbie

ACS Nano, **Just Accepted Manuscript** • DOI: 10.1021/acsnano.5b02676 • Publication Date (Web): 08 Sep 2015

Downloaded from <http://pubs.acs.org> on September 9, 2015

Just Accepted

“Just Accepted” manuscripts have been peer-reviewed and accepted for publication. They are posted online prior to technical editing, formatting for publication and author proofing. The American Chemical Society provides “Just Accepted” as a free service to the research community to expedite the dissemination of scientific material as soon as possible after acceptance. “Just Accepted” manuscripts appear in full in PDF format accompanied by an HTML abstract. “Just Accepted” manuscripts have been fully peer reviewed, but should not be considered the official version of record. They are accessible to all readers and citable by the Digital Object Identifier (DOI®). “Just Accepted” is an optional service offered to authors. Therefore, the “Just Accepted” Web site may not include all articles that will be published in the journal. After a manuscript is technically edited and formatted, it will be removed from the “Just Accepted” Web site and published as an ASAP article. Note that technical editing may introduce minor changes to the manuscript text and/or graphics which could affect content, and all legal disclaimers and ethical guidelines that apply to the journal pertain. ACS cannot be held responsible for errors or consequences arising from the use of information contained in these “Just Accepted” manuscripts.



Enhanced Luminescent Stability through Particle Interactions in Silicon Nanocrystal Aggregates

Joseph B. Miller,^{†,§} Naveen Dandu,[†] Kirill A. Velizhanin,[§] Rebecca J. Anthony,^{‡,¶} Uwe R. Kortshagen,[‡] Daniel M. Kroll,[†] Svetlana Kilina,[†] and Erik K. Hobbie^{*†}

[†] North Dakota State University, Fargo, North Dakota 58108

[§] Theoretical Division, Los Alamos National Laboratory, New Mexico 87545

[‡] University of Minnesota, Minneapolis, Minnesota 55455

RECEIVED DATE ()

ABSTRACT: Close-packed assemblies of ligand-passivated colloidal nanocrystals can exhibit enhanced photoluminescent stability, but the origin of this effect is unclear. Here, we use experiment, simulation and *ab initio* computation to examine the influence of inter-particle interactions on the photoluminescent stability of silicon nanocrystal aggregates. The time-dependent photoluminescence emitted by structures ranging in size from a single quantum dot to agglomerates of more than a thousand is compared with Monte Carlo simulations of non-interacting ensembles using measured single-particle blinking data as input. In contrast to the behavior typically exhibited by the metal chalcogenides, the measured photoluminescent stability shows an enhancement with respect to the noninteracting scenario with increasing aggregate size. We model this behavior using time dependent density-functional theory calculations of energy transfer between neighboring nanocrystals as a function of nanocrystal size, separation, and the presence of charge and/or surface-passivation defects. Our results suggest that rapid exciton transfer from ‘bright’ nanocrystals to surface trap states in nearest-neighbors can

1
2
3 efficiently fill such traps and enhance the stability of emission by promoting the radiative
4
5 recombination of slowly diffusing excited electrons.
6
7

8
9
10 KEYWORDS: silicon nanocrystals, fluorescence intermittency, nanocrystal interactions, energy
11
12 transfer
13
14
15

16
17 The tunable emission enabled by quantum confinement imparts semiconductor nanocrystals
18
19 with a unique band-gap photoluminescence that shows considerable promise for fluorescent
20
21 tagging and sensing applications.^{1,2} By far, the most widely and deeply studied materials in this
22
23 regard have been the metal chalcogenides such as CdSe, which offer excellent quantum yield,
24
25 broad color access, fast lifetime, narrow line width and improved photoluminescent stability over
26
27 conventional fluorophores.³ Although such materials are commercially available, easily endowed
28
29 with specific biochemical functionality and are presently being used with a remarkable degree of
30
31 effectiveness, an element of uncertainty regarding the potential toxicity of the metal
32
33 chalcogenides⁴⁻⁶ has generated a significant amount of activity directed at finding nontoxic earth-
34
35 abundant alternatives. In this regard, nanocrystalline silicon has emerged as a material of
36
37 considerable current interest.
38
39
40
41

42
43 Silicon nanocrystals (SiNCs) synthesized through a variety of plasma-assisted⁷⁻¹¹ or solution-
44
45 based¹²⁻¹⁷ chemistries exhibit tunable photoluminescence (PL) across the visible to the near-
46
47 infrared.¹⁶⁻²⁰ Once imparted with colloidal stability through ligand passivation or other surface
48
49 treatment, SiNCs can be separated by size to yield monodisperse colloidal suspensions.²¹⁻²⁴ In
50
51 terms of PL, the potential utility of these materials has already been demonstrated for a range of
52
53 bioimaging²⁵⁻²⁷ and responsive polymer nanocomposite²⁸⁻³⁰ applications. Nonetheless, there are a
54
55 number of unresolved questions related to the role of surface states,³¹ the interplay of quantum
56
57
58
59
60

1
2
3 confinement and the indirect band gap of silicon,³² and the impact of particle interactions on
4 photoluminescence.^{33,34} In terms of the latter, an intriguing trait recently reported for nanocrystal
5
6 ‘solids’ assembled from colloidal SiNCs is an ensemble brightening under continuous excitation,
7
8 where the emission and PL lifetime exhibit a temporal increase instead of the usual
9
10 photobleaching.²¹ Similar behavior has also been observed in the metal chalcogenides, where it
11
12 has been attributed to dark-state passivation mediated by mobile photo-excited electrons.³⁵ In a
13
14 much broader view, energy transfer from nanocrystals to polymers, dye molecules, or other
15
16 acceptors is a topic of considerable current interest.³⁶⁻³⁹
17
18
19
20
21

22 A fundamental understanding of such phenomena must start with the smallest distinct
23
24 element; the emission from an individual nanocrystal. Like all fluorophores, semiconductor
25
26 nanocrystals exhibit fluorescence intermittency or ‘blinking’, whereby the PL randomly switches
27
28 between bright (*on*) and dark (*off*) states.⁴⁰⁻⁴⁶ The *off* state of a semiconductor nanocrystal has
29
30 commonly been associated with charge/ionization states and subsequent Auger-assisted
31
32 recombination. However, recent insight from controlled electrochemical studies on CdSe
33
34 suggests two distinct blinking mechanisms; a charging/decharging of the nanocrystal core -
35
36 where low PL correlates with shorter lifetime - and a second mechanism in which electron-
37
38 accepting surface states intercept ‘hot’ electrons before they can radiatively relax into the core.⁴²
39
40 These are delineated A-type and B-type blinking, respectively. Interestingly, both mechanisms
41
42 can be electrochemically suppressed by the application of an appropriate potential.⁴² An even
43
44 higher level of complexity is suggested by the recent observation that the emission time trace of
45
46 a single nanocrystal is not just binary, but can be multileveled in a manner that reflects the
47
48 potentially complex energy landscape of surface trap states.⁴⁷ A significant amount of
49
50
51
52
53
54
55
56
57
58
59
60

1
2
3 information related to nanocrystal blinking and photostability is thus contained in the time
4
5 dependent emission.⁴⁸⁻⁵⁵
6
7

8 Here, we use experiment, simulation and *ab initio* computation to examine the influence of
9
10 inter-particle interactions on the photoluminescent stability of SiNC aggregates. To the best of
11
12 our knowledge, this is the first in-depth study of the blinking behavior of ligand-stabilized
13
14 colloidal SiNCs, either as individuals or as a collective. The time-dependent PL emitted by
15
16 structures ranging in size from an isolated SiNC up to dense assemblies containing thousands of
17
18 nanocrystals is measured at varied excitation power and particle-size homogeneity.
19
20 Measurements as a function of aggregate size are compared with Monte Carlo simulations of
21
22 non-interacting ensembles that employ measured single-particle blinking data as input. In
23
24 contrast to the behavior typically observed for CdSe, we find a significant stabilizing effect with
25
26 respect to the noninteracting scenario, which we model using density-functional theory (DFT)
27
28 calculations of energy transfer between neighboring nanocrystals as a function of SiNC size,
29
30 separation, and the presence of charge and/or surface defects. Our results suggest that rapid
31
32 exciton transfer from ‘bright’ nanocrystals to trap states in nearest-neighbors can efficiently fill
33
34 such traps and enhance the PL stability by promoting the radiative relaxation of slowly diffusing
35
36 excited electrons.
37
38
39
40
41
42
43
44
45

46 **Results and Discussion**

47
48 We consider both a parent material (denoted AP) and a monodisperse fraction (denoted F) of
49
50 comparable mean size (4 nm) as determined by transmission electron microscopy (TEM). Both
51
52 have peak PL emission near 750 nm and a particle size in the vicinity of the exciton Bohr radius
53
54 of silicon.²¹ Blinking as a function of time was measured over long intervals with large
55
56
57
58
59
60

ensembles for each sample type (F vs. AP) at both low (LP, 140 W/cm²) and high (HP, 5000 W/cm²) power under 473 nm CW excitation. Although a single emitter can be identified through photon antibunching in the PL intensity autocorrelation function,³⁸ we seek to discriminate intensity as a function of aggregate size over very long time scales and thus benefit from a different approach that relies on real-space verification of the size of the emitter. Some typical results are shown in Fig. 1. The smallest resolvable feature in AFM was identified to be a single SiNC by using successively smaller AFM scans while deconvolving the contribution of the tip profile from the height signal. Details are given in the Supporting Information.

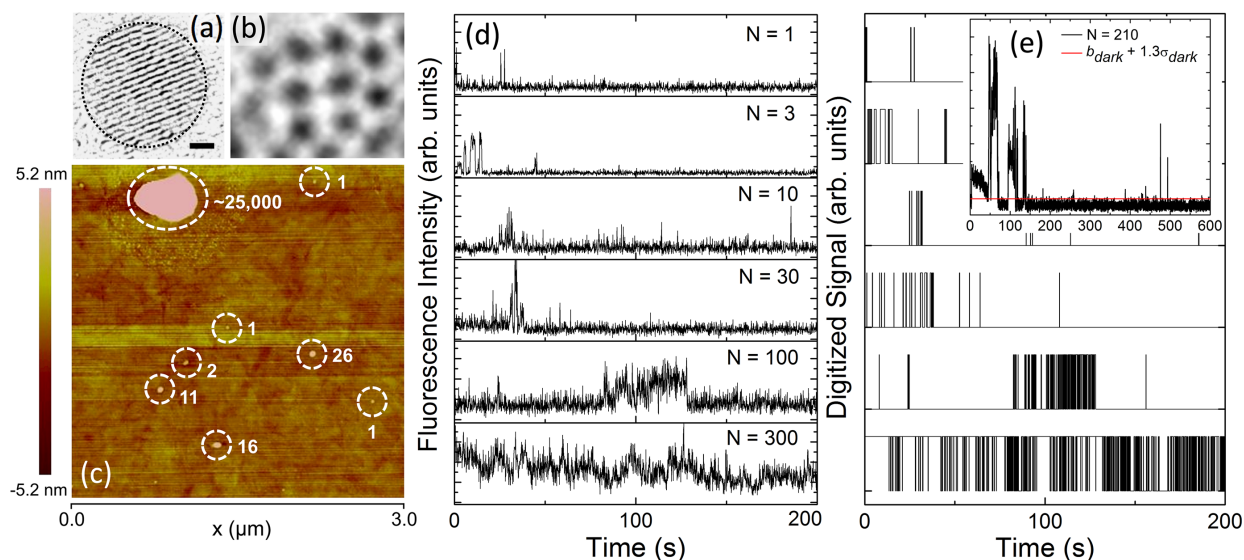


Figure 1: (a) TEM image of a single SiNC (1 nm scale). (b) TEM image of a packed assembly of monodisperse 4 nm diameter SiNCs. (c) AFM scan showing SiNCs clusters of varied size, including a large cluster used as a coordinate reference point. (d) Typical time-dependent PL traces collected for varied N . (e) Binary fluorescent signals from panel (d) based on an intensity threshold as depicted in the inset for $N \approx 200$.

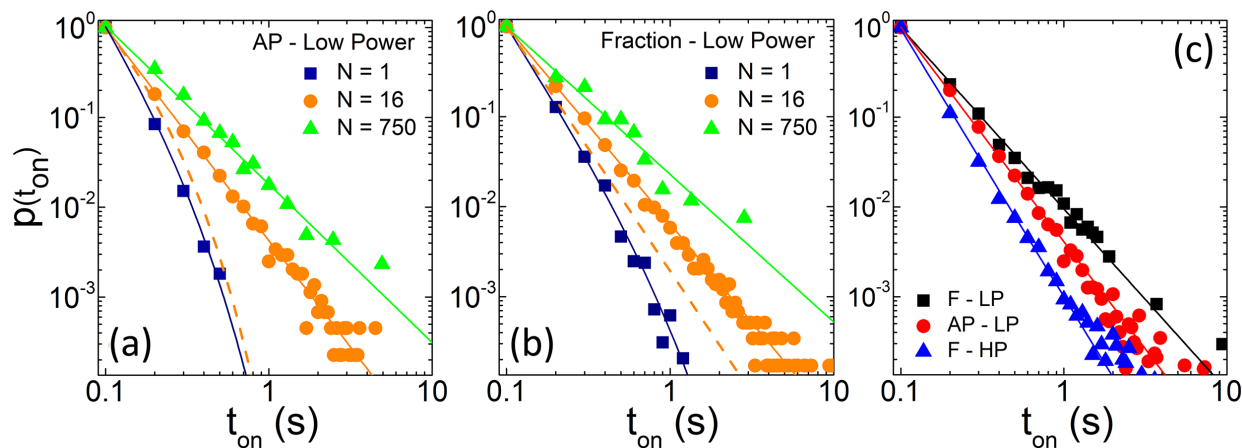


Figure 2: (a) *On* time statistics for a collection of as-produced (AP) SiNC aggregates of size $N = 1, 16$ and 750 at low excitation power and (b) a similar plot obtained for a monodisperse fraction (F). The dashed curves in (a) and (b) are the $N = 16$ distributions tabulated from 16 independent $N = 1$ blinking traces. (c) *On* time statistics for the monodisperse fraction and AP material at low excitation power and the fraction at high power, where the data include all N . Distributions are normalized to $p = 1$ at $t_{\text{on}} = 0.1$ s.

Typical blinking sequences are shown in Fig. 1d for a range of emitter size. For an accessible description of the *on-off* statistics in light of the complex emission dynamics anticipated for an aggregate, we first render these time traces into binary *on/off* sequences in the usual way through a threshold intensity set to exclude background noise. Examples can be found in Fig. 1d & e. The equivalent binary waveform then yields *on* and *off* statistics, as shown in Fig. 2 for the *on* times under a variety of conditions. Additional distributions are shown in the Supporting Information. The distributions are mostly power-laws, with a small number of truncated power-laws of the form $p(t) \propto t^{-\alpha} \exp(-t/\tau)$. A table of the relevant fitting parameters is given in the Supporting Information (Table S1 & S2). The exponent α decreases with increasing N and varies between 1.5 and 3, where the larger end is likely influenced by uncertainties associated with the cutoff.

For single-nanocrystal emission, the nature of such power-laws has been shown to depend on the precise choice of threshold and binning.⁵⁶⁻⁵⁷ Although this is not a critical issue for the brighter aggregates, we nonetheless avoid relying exclusively on these fitting parameters to draw meaningful conclusions. In Fig. 2a & b, the dashed curve for $N = 16$ is the behavior obtained by summing 16 single-dot ($N = 1$) time traces, which is well below the measured *on*-time distribution for $N = 16$.

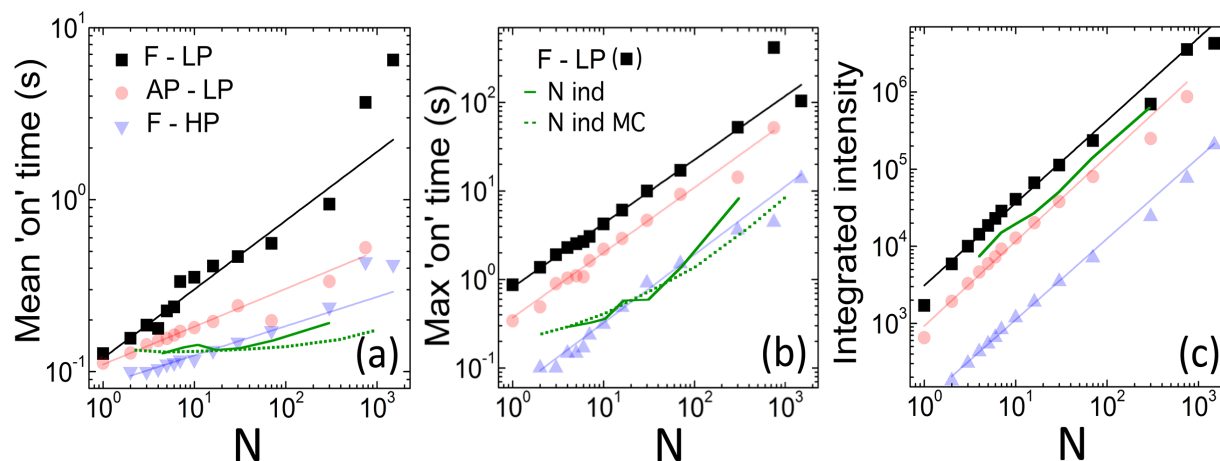


Figure 3: (a) The mean *on* time, (b) the maximum *on* time, and (c) the integrated intensity as a function N . In each panel, the green curves are the equivalent quantity computed from the appropriate number of individual ($N = 1$) SiNCs for the fraction at low power (F-LP) based on both measurement (solid) and MC simulation (dashed).

The various moments of these distributions (Fig. 3) are revealing and typically scale in a power-law fashion as N^β , where a table of the exponents can be found in the Supporting Information (Table S3) along with additional quantities (Fig. S6, Supporting Information). The general trends are better stability and longer *on* time at lower excitation power and lower size disparity. Focusing on the fraction at low power, we can again compare the measured behavior with that anticipated for N independent single emitters (green curves, Fig. 3) which now includes

1
2
3 both Monte Carlo (MC) simulations (dashed green) and the behavior obtained by summing N
4 measured single SiNC time sequences (solid green). The MC simulations are indeed consistent
5
6 with the integrated $N = 1$ experimental results, but both differ from the measured behavior, as
7
8 can be seen by comparing the green curves (no interactions) with the black curves (measured) in
9
10 Fig. 3. This difference is most meaningful for the average *on* time (Fig. 3a) since the maximal
11
12 values will depend on the particular measured $N = 1$ traces chosen for size integration.
13
14
15
16

17
18 With the exception of Fig. 3a, the exact values of the exponents in the power-law trends do
19
20 not vary drastically with excitation power or size homogeneity, but there are large differences in
21
22 the amplitude of the effect. The behavior at higher excitation power reflects the fact that we are
23
24 operating in a regime of very few emitters compared to the number of incident photons, and
25
26 more emitters are thus being driven into dark states at higher photon flux through rapid and
27
28 repeated excitation. In terms of interaction effects, the data in Figs. 2 & 3 suggest that aggregates
29
30 are more stable than the same number of individuals regardless of size distribution. On top of
31
32 this, however, the data suggest that such interaction effects are enhanced for narrower size
33
34 distributions (Fig. 3a).
35
36
37
38

39
40 As detailed in Fig. 4, the same trends can be seen in the autocorrelation function of the time
41
42 dependent emission; $c(t) = \langle I(t')I(t'+t) \rangle / \langle I(t')I(t') \rangle$ where the brackets denote an average over t' .
43
44 This is determined directly from the background-corrected PL intensity and is thus independent
45
46 of *on/off* binning or binarization.⁵⁸ For each N in Fig. 4, the data represent an average over many
47
48 features of identical (for $N = 1$ and small N) or comparable mean (for much larger N) size. For
49
50 small N , $c(t)$ decays to zero with increasing time because there is no long- t correlation in the
51
52 intensity. For large N , the abrupt late- t cutoff reflects the finite size of the sampling interval, and
53
54 we thus limit our quantitative analysis to $t < 10 \cdot 10^2$ s. Figures 4a-b suggest a correlation time that
55
56
57
58
59
60

1
2
3 increases with increasing aggregate size and decreasing power, which we quantify by first
4
5 considering projections of $c(t)$ onto the N axis at varied time. All such projections can be scaled
6
7 onto a single master curve by defining a time-dependent critical size, $N_c(t)$, as shown in Fig. 4d
8
9 & e. All scenarios show the same power-law dependence; $N_c \propto t^\gamma$ with $0.9 < \gamma < 1$. What differs
10
11 is the proportionality constant, which increases by a factor of 3 from F-LP to AP-LP and by
12
13 nearly a factor of 40 from F-LP to F-HP. Physically, N_c is the minimum size exhibiting emission
14
15 stability over a time interval t . For long time intervals, only clusters much larger than N_c exhibit
16
17 stable emission. This is evident in the Fourier transform of $c(t)$ [the spectral power density,
18
19 $S(\omega)$], which exhibits a low-frequency divergence for the largest N (Fig. 4f, F-LP). The linearity
20
21 of N_c as a function of time is also evident in logarithmic intensity plots of $c(t)$ in the t - N plane,
22
23 as shown in Fig. 5a-c.
24
25
26
27
28
29
30
31

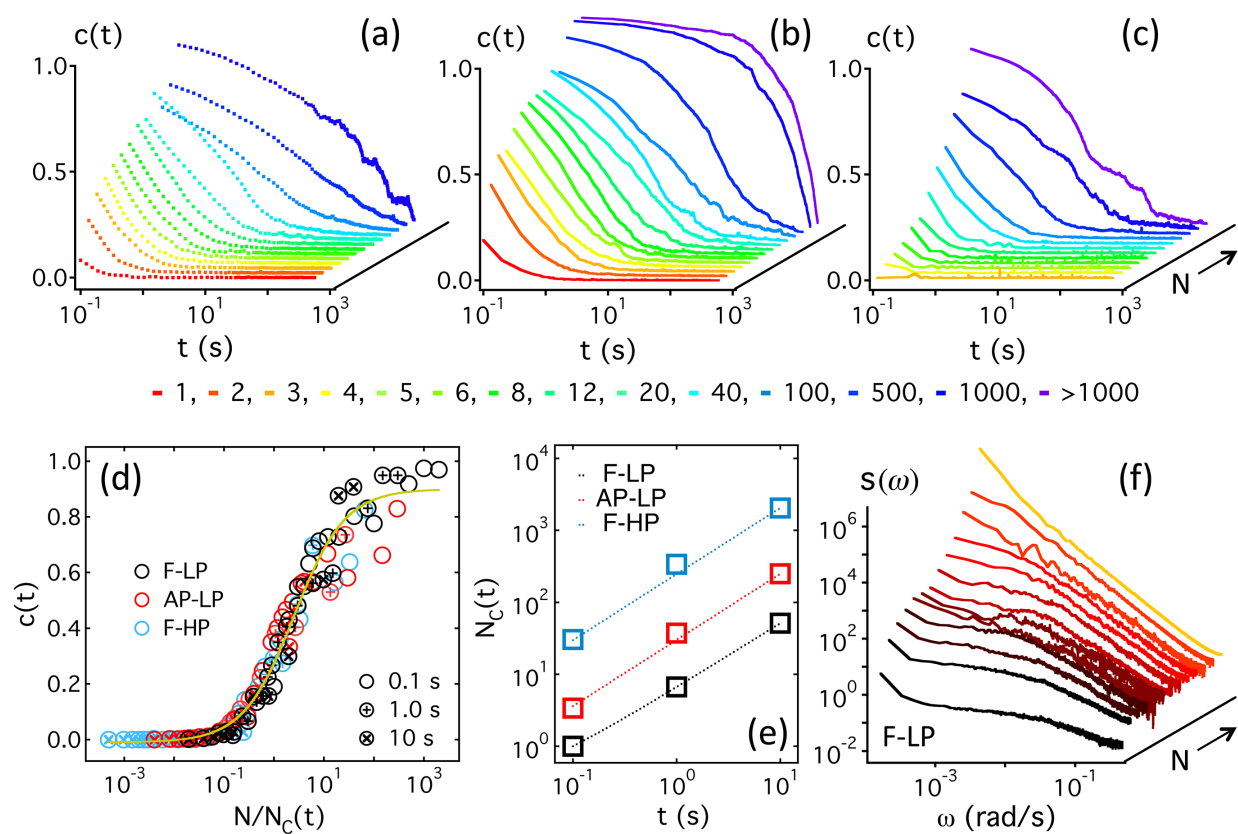


Figure 4: Fluorescence autocorrelation function $c(t)$ as a function of N for (a) the as-produced (AP) material under low excitation power, (b) the fraction (F) under low excitation power and (c) the fraction under high excitation power. The color legend for N is shown below the graphs. (d) Scaling plot of the N -dependence of $c(t)$ for each scenario at the indicated times (0.1 s, 1.0 s and 10 s) in terms of a single time-dependent scaling parameter N_c . (e) The time dependence of N_c for each scenario and (f) the N dependence of $S(\omega)$ for the F-LP data shown in panel (b).

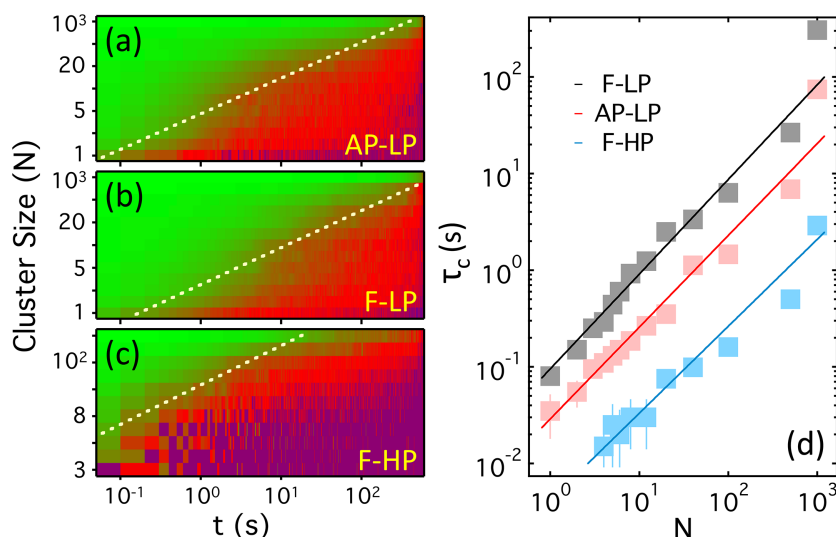


Figure 5: Log intensity plots of $c(t)$ in the plane of size and time for (a) AP-LP, (b) F-LP, and (c) F-HP. The lines indicate linear time dependence, where deviations from this trend are due to a distribution of sizes that is not perfectly logarithmic. (d) Correlation time vs. size with power-law fits that are close to linear (exponents from 0.9 to 0.98). Data for $\tau_c < 100$ ms are interpolated from spline fits down to $c(0) = 1$.

The results of Fig. 4e and Fig. 5 are revealing. The spin-coating process creates assemblies that tend to be coplanar (Fig. 1c), so there is a simple average relationship between cluster size, N , and cluster length scale, R , with $N \propto R^2$. Figure 4e shows that N_c is nearly linear in time, which implies $R_c^2 \approx 4Dt$ with a diffusion coefficient, D , given by the proportionality constant in

1
2
3 Fig. 4e. Specifically, we find $D \approx 10 \text{ nm}^2/\text{s}$ (F-LP), $45 \text{ nm}^2/\text{s}$ (AP-LP) and $370 \text{ nm}^2/\text{s}$ (F-HP). The
4
5 increase in D between F-LP and F-HP ($\sim 35\times$) mirrors the increase in excitation power, implying
6
7 that the diffusion coefficient is proportional to fluence. Because $c(t)$ obtained from a sum of N
8
9 single ($N = 1$) emitters does not show this enhanced correlation (Fig. S7, Supporting
10
11 Information), we further infer that $N_c(t)$ is determined by SiNC interactions. Diffusion-
12
13 controlled processes have previously been identified in the blinking of CdSe nanocrystals,⁴³ but
14
15 to our knowledge this is the first time they have been reported for silicon. Here, we note that the
16
17 scaling in Fig. 4d implies an analogous scaling in terms of $t/\tau_c(N)$, where $\tau_c \propto N/D \propto R^2/D$ is
18
19 a correlation time. Fits of τ_c (the time required to decay to $1/e$) as a function of N are shown in
20
21 Fig. 5d. The physical interpretation of projecting the data in this manner is that aggregates in an
22
23 *on* state at $t = 0$ are still likely to be *on* at $t = \tau_c$, where τ_c increases nearly linearly with size. A
24
25 final piece of insight comes from the supporting movies, which show that aggregates turn *off*
26
27 abruptly (faster than $\sim 100 \text{ ms}$). This implies that the temporal decay of $c(t)$ at fixed N arises
28
29 from a statistical superposition of different *on* times and not from a gradual *on-off* transition.
30
31
32
33
34
35
36

37 Taken collectively, the experimental data reveal some important and surprising trends. First
38
39 and foremost, SiNC aggregates exhibit enhanced PL stability, regardless of the magnitude of the
40
41 excitation power or the narrowness of the size distribution. The causal role of defects,⁵⁹⁻⁶¹ surface
42
43 trap states,⁶²⁻⁶⁵ and charge⁶⁶⁻⁷² in the PL intermittency of quantum dots is well documented, and
44
45 the logical conclusion is that nearest neighbor SiNCs ‘passivate’ each other by reducing the
46
47 collective number of surface trap states available to the ensemble. An attractive way to explain
48
49 this would be through a transfer scheme in which excitons from a ‘bright’ nanocrystal occupy the
50
51 trap states of a ‘dark’ neighbor. Second, higher excitation power reduces but does not eliminate
52
53 this collective trend. The higher the flux of incident photons, the more frequently a given
54
55
56
57
58
59
60

1
2
3 nanocrystal will be excited across the band gap and the more likely the relaxing electron will
4
5 encounter a trap state, but nearest neighbors still provide a stabilizing effect. Third, size disparity
6
7 reduces this collective enhancement through disorder in the band-gap energy, which has been
8
9 shown to slow down exciton transport through close-packed lattices.⁷³
10
11

12
13 Although the above ideas are intuitive, they require a computational foundation. Toward this
14
15 end, we used time-dependent DFT (TD-DFT) to compute inter-SiNC energy-transfer rates for
16
17 scenarios relevant to the experiments. A DFT-based approach was recently used to study the role
18
19 of dangling-bond defects in the blinking behavior of individual oxidized SiNCs.⁷⁴ These studies
20
21 confirm the presence of hot-electron traps in oxidized SiNCs, which are important for B-type
22
23 blinking. While this approach⁷⁴ treats an excitation as an unbound electron-hole pair, recent
24
25 calculations⁷⁵ show that excitonic effects are much stronger in SiNCs than in bulk Si, and they
26
27 cannot be neglected for energy transfer calculations. In addition, it has been shown⁷⁶ that
28
29 multipolar terms dominate the Coulomb coupling when the distance between nanocrystals is
30
31 smaller than 2 nm. Our approach to energy transfer thus includes both excitonic effects and
32
33 multipole terms in the Coulomb integral for the coupling between neighboring SiNCs.
34
35
36
37
38
39
40
41
42
43
44
45
46
47
48
49
50
51
52
53
54
55
56
57
58
59
60

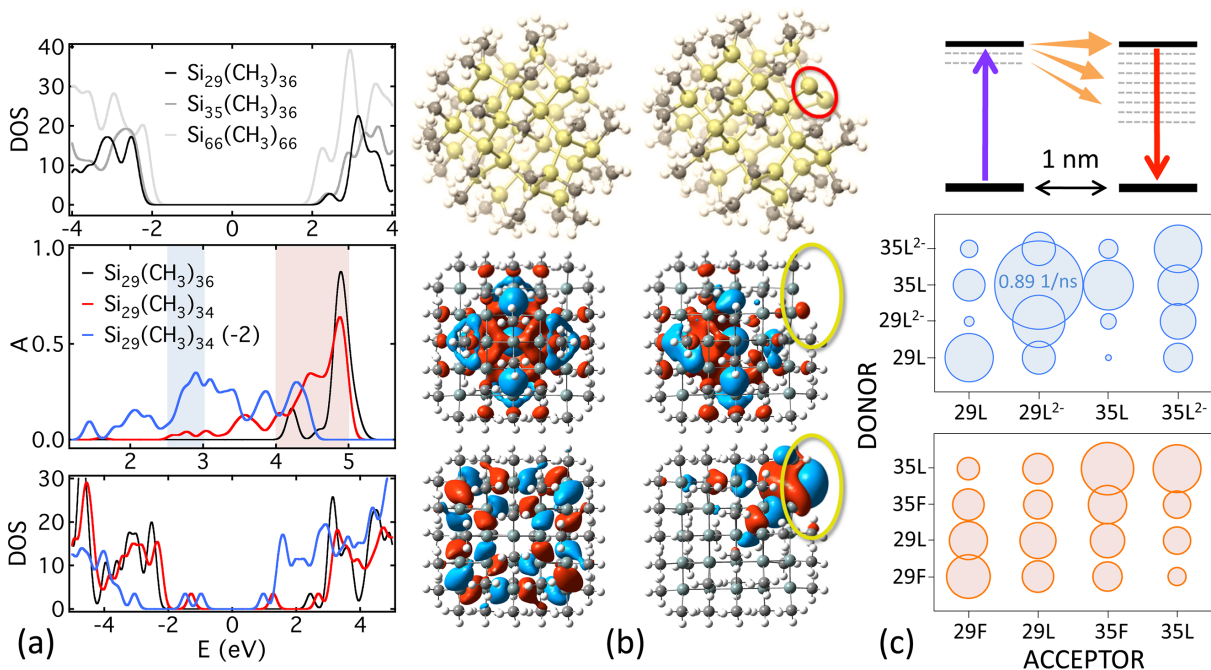


Figure 6: (a) (top) Computed DOS for varied SiNC size; (middle) absorbance for defect-free Si_{29} (black), with 2 ligands removed (red), and with 2 missing ligands and -2 charge (blue); (bottom) Computed DOS for the scenarios in the middle panel, where energy is the horizontal axis in all three plots. (b) Simulated structures for (left) defect-free Si_{35} and (right) the L^{2-} configuration (2 missing ligands + 2 electrons) (top) and the excited orbital (NTO) for an electron (middle) and hole (bottom). The defect is located in the top right corner. (c) (top) Band diagram for energy transfer from a 'bright' SiNC to a 'dark' (defective) SiNC and (bottom) area-based bubble charts of k_{ET} for a variety of donor/acceptor pairs at 1 nm separation. The blue data (middle) consider the effect of a missing ligand and charge while the red data (bottom) consider the effect of only a missing ligand, where the common bubble scale is indicated for the highest rate. Blue/red data are excited at the blue/red region in (a).

The SiNCs were modeled as Si clusters with a bulk-diamond structure. We consider 29 Si atoms (1.2 nm diameter), 35 Si (1.35 nm diameter) and 66 Si (1.6 nm diameter). Methane ligands

1
2
3 were covalently bonded to the surface Si atoms to passivate dangling bonds. The fully passivated
4 structures are denoted F, but we also simulated defective SiNCs by removing a ligand from each
5
6 of the two nearest 3-coordinated Si atoms (denoted L) and charged structures with ± 2 charge
7
8 introduced on both fully passivated ($F^{2\pm}$) and defective ($L^{2\pm}$) SiNCs. Förster resonant energy
9
10 transfer (FRET) rates k_{ET} were then calculated between different SiNC donor/acceptor pairs at
11
12 varied separation based on the DFT transition density matrix. As shown in the top panel of Fig.
13
14 6a, the band gap under full passivation exhibits quantum confinement. The presence of surface
15
16 defects and surface charge leads to trap states within the gap (bottom panel, Fig. 6a), resulting in
17
18 the appearance of red-shifted dark and semi-dark optical transitions in the absorption spectra, as
19
20 shown in the middle panel of Fig. 6a. Additional calculations can be found in the Supporting
21
22 Information. Figure 6b shows the varied structure of the Si_{35} nanocrystal for both the fully
23
24 passivated scenario (left) and for a charged defect (right, 2 missing ligands with 2 surface
25
26 electrons). The top panel is the structure and the middle panel shows the natural transition orbital
27
28 (NTO) for an excited electron and a hole contributing to the lowest energy optical transition,
29
30 illustrating an increase in the localization of the electron-hole density around the defect, which
31
32 decreases the oscillator strength of such transitions. A schematic of the transfer scenario and the
33
34 computed k_{ET} for a variety of scenarios are shown in Fig. 6c. In the middle panel, the excitation
35
36 is implemented over the optically weak lower energy band - marked by blue in Fig. 6a and
37
38 present only in charged and defective SiNCs - while in the lower panel the excitation involves
39
40 the most optically active band, marked by red in Fig. 6a.
41
42
43
44
45
46
47
48
49

50 The energy transfer rate between neighboring SiNCs decays strongly with distance while
51
52 multipole contributions are crucial for separations near 1 nm (particularly when photoexcitation
53
54 involves optically-weak lower-energy transitions, with more than an order of magnitude
55
56
57
58
59
60

1
2
3 difference in k_{ET} between dipole-dipole and multipole approaches - Supporting Information,
4 Fig. S10). At the fixed separation of 1 nm in Fig. 6, it depends on two factors; the transition
5 dipole moment of the donor/acceptor and the DOS of the acceptor at the excitation energy of the
6 donor; k_{ET} is maximized when both are optimal. Indeed, these conditions are satisfied when the
7 donor and acceptor have identical structure, as observed in most of the scenarios in Fig. 6c (a few
8 exceptions to this rule are discussed in the Supporting Information). This is consistent with the
9 experimental observation of enhanced PL stability in the size-purified fraction and supports the
10 hypothesis of band alignment through band-gap homogeneity. The calculated k_{ET} are two-
11 orders-of-magnitude faster than the radiative recombination rates that we compute from TD-DFT
12 (Supporting Information). Within the DFT framework, energy transfer is thus efficient on the
13 scale of 10 ns, even for states with low oscillator strength (semi-dark trap states), which provides
14 an additional channel for occupying the lowest-lying dark or semi-dark states. For phonon-
15 induced relaxation, energy transfer thus facilitates the occupation of nonradiative trap states,
16 which would increase the stability of PL from optically bright states associated with the
17 nanocrystal core. This, in turn, would lead to an increase in the average *on* time for densely
18 packed SiNC ensembles, consistent with the experiments.

19
20
21
22
23
24
25
26
27
28
29
30
31
32
33
34
35
36
37
38
39
40
41
42
43
44
45
46
47
48
49
50
51
52
53
54
55
56
57
58
59
60
Previous work on the blinking of isolated nanocrystals suggests significant differences
between silicon and CdSe.^{48,77-79} In particular, a B-type blinking mechanism in SiNCs has been
associated with the activation/deactivation of a nonradiative recombination center associated
with dangling surface bonds.⁷⁴ Type B blinking arises when ‘hot’ electrons get caught in surface
trap states and are unable to recombine with a hole.^{42,74} Here, the linear scaling of τ_c with N can
be explained by a simple tentative argument that bridges the experiments to the DFT. To identify
a characteristic time scale, we model the quantum yield of an aggregate as

$$\Phi \approx \frac{k_R + \xi k_{ET}}{k_R + k_{NR} + k_{ET}} \quad (1)$$

where k_R is the radiative rate constant, k_{NR} is the nonradiative rate constant, k_{ET} is the rate constant associated with energy transfer (assumed to be the fastest channel present) and the parameter ξ sets the balance between radiative and nonradiative effects associated with energy transfer. Assuming the slow process of interest resides in the nonradiative channel, the rate of change is $\dot{\Phi} \approx -\xi \dot{k}_{NR}/k_{ET}$.

We further hypothesize that k_{NR} is proportional to the concentration of hot electrons, φ , which is proportional to the excitation power, p . The lower number of nearest-neighbor SiNCs at the aggregate boundary means that energy transfer will be less efficient there, implying that there will be more unoccupied trap states at the edge. Diffusion then implies $\dot{k}_{NR} \propto \partial\varphi/\partial t \propto D_0\varphi/R^2$ where D_0 is a bare diffusion coefficient of hot electrons, which gives $\dot{\Phi} \propto k_{ET}^{-1}D_0\varphi/R^2 \propto k_{ET}^{-1}D_0\varphi/N \propto \tau_c^{-1}$, or $\tau_c \propto N/D_{eff}$ with an effective diffusion coefficient $D_{eff} \propto \varphi D_0/k_{ET} \propto pD_0/k_{ET}$. This increases linearly with power (in agreement with the experiments) and is inversely proportional to k_{ET} . At equal excitation power, the experiments give $D_{AP}/D_F \approx 3$, which would imply $(k_{ET})_F/(k_{ET})_{AP} \approx 3$. This can be compared with the ratio of the average k_{ET} for identical and different sizes in Fig. 6c (~ 2.2 excluding the 35L-29L²-outlier), where the difference might reflect other variables such as excess ligand in the parent. The magnitude of D (10^{-13} to 10^{-11} cm²/s) is comparable to the diffusion coefficient of electrons in polyethylene,⁸⁰ suggestive of diffusion in the ligand shell, although more work is needed to fully understand this intriguing slow process. The physical picture that emerges is thus the diffusion-controlled accumulation of hot electrons in traps at the boundary, which eventually

1
2
3 causes the agglomerate to abruptly turn *off* when exciton transfer can no longer compensate for
4
5 the increasing number of trapped electrons.
6
7

8 Previous in-depth studies of the PL intermittency from SiNCs have focused on single
9 emitters in noncolloidal structures,⁷⁷⁻⁷⁹ but the influence of nanocrystal interactions on the
10 blinking of SiNC aggregates has not been previously considered for any type of SiNC.
11 Interaction effects have been investigated for colloidal CdSe quantum dots and nanorods,⁸¹⁻⁸⁵
12 while a handful of other papers have examined energy transfer from a nanocrystal to a dissimilar
13 object, such as a dye molecule,^{36,86} graphene,³⁷ a conjugated polymer,³⁸ or a nearby surface.³⁹ In
14 general, such work suggests that interaction effects and/or energy transfer give rise to faster
15 blinking rates or suppressed nanocrystal *on* times, which is the opposite of what we observe here.
16
17 One exception is the work of Wang *et al.* on core/double-shell CdSe nanorods,⁸² who found
18 enhanced *on* times without any discernable interaction effects in the *off* times. On one level, this
19 suggests that there must be something unique about the double-shell CdSe nanorod structures
20 with respect to other CdSe nanocrystals. More relevant to the point of this study, it suggests that
21 nanocrystal interactions have a clear beneficial effect on the PL stability of colloidal SiNC
22 assemblies.
23
24
25
26
27
28
29
30
31
32
33
34
35
36
37
38
39

40 Finally, we explain the different magnitude of the effect apparent in the mean *on* time (Fig.
41 3a) compared to the integrated intensity (Fig. 3c). In simple terms, the mean *on* time is the total
42 *on* time (Fig. S6a, Supporting Information) divided by the total number of blinking events in an
43 observation interval. The sub-linear N -dependence of the mean *on* time in Fig. 3a implies that the
44 number of such blinking events increases with N , but not as fast as the total *on* time. This is
45 intuitive, since the number of such events should increase with the number of emitters. The
46 difference in total *on* time between N and the sum of N individuals is rather modest (Fig. S6a,
47
48
49
50
51
52
53
54
55
56
57
58
59
60

1
2
3 Supporting Information), which implies that the temporal density of blinking events must
4
5 increase more strongly with N in the noninteracting scenario; N individuals blink more often than
6
7 an aggregate, or the latter exhibit better PL stability.
8
9

10
11 The integrated intensity, in contrast, is just the summed intensity of each time frame. This
12
13 can be trivially coarse-grained to $\sum_j I_j$, where the index j corresponds to a single blinking event
14
15 and I_j is the total intensity of the event. The integrated intensity is thus proportional to the total
16
17 number of blinking events multiplied by the average intensity per event, with the data in Fig. 3c
18
19 suggesting that the integrated intensity is proportionally to N for both the interacting and
20
21 noninteracting scenarios. From the mean *on* time discussed above, however, we know that the
22
23 number of blinking events increases more strongly with N for the integrated $N = 1$ results, which
24
25 implies that the total intensity per blinking event increases more slowly. In terms of the N -
26
27 dependence with and without interactions, the intensity-related quantity that is analogous to
28
29 mean *on* time is thus the mean total intensity per blink, which is enhanced due to the enhanced
30
31 stability associated with interactions. We note that the data also suggest that the constant of
32
33 proportionality in Fig. 3c is slightly smaller for the integrated $N = 1$ results, since the difference
34
35 in amplitude is outside of the uncertainty (a roughly 20 % combined uncertainty compared to a
36
37 40 % difference based on purely linear fits through the origin). This is a much smaller effect,
38
39 however, that is closer to the resolution limit of the experiments.
40
41
42
43
44
45
46
47

48 **Conclusions**

49
50 In conclusion, we have used experiment, simulation and *ab initio* computation to examine the
51
52 role of inter-particle interactions on the PL stability of colloidal SiNC aggregates. In contrast to
53
54 the behavior typically reported for CdSe, the measured stability as a function of increasing
55
56
57
58
59
60

1
2
3 collective size shows an enhancement with respect to the noninteracting scenario. We have
4 modeled this behavior using time-dependent DFT calculations of energy transfer between
5 neighboring nanocrystals in the presence of charge and/or surface-passivation defects. Our
6 results suggest that rapid energy transfer - or more precisely, exciton transfer^{75,87} - from 'bright'
7 nanocrystals to 'dark' trap states in nearest-neighbors can efficiently fill such trap states and
8 improve the stability of aggregate emission. Although a rigorous theoretical accounting extended
9 to larger SiNC sizes is still needed, this mechanism gives us one possible foundation for a more
10 quantitative explanation of how nanocrystal interactions improve the PL stability of aggregates.
11
12
13
14
15
16
17
18
19
20
21

22 Focusing on the autocorrelation data, our results can be interpreted in terms of a fluence-
23 dependent slow diffusion of hot electrons that is tempered by particle interaction effects. Just as
24 an individual SiNC abruptly transitions to the *off* state when an electron gets caught in a surface
25 trap state, an aggregate abruptly turns *off* when a sufficient number of 'hot' electrons have found
26 unoccupied trap states. In our model, these trap states have a higher density at the boundary
27 where the energy transfer scheme is less efficient. It would thus take longer for this to happen for
28 larger N , since it requires the slow diffusion of electrons to the boundary. Modeling these
29 interaction effects using time-dependent DFT yields predictions that are qualitatively supported
30 by the data.
31
32
33
34
35
36
37
38
39
40
41
42

43 The results make sense intuitively, given the critical role of surface passivation in the PL of
44 SiNCs. At these excitation powers, we typically observe that a single SiNC is more likely to
45 exhibit short *on* times. Only in the presence of other nanocrystals do these *on* times begin to
46 become appreciable. We suspect that this has something to do with the dried state of the colloidal
47 SiNCs, as we measured the quantum yield of the nanocrystal solutions just prior to these
48 measurements and found the anticipated results.^{8-11,21} One possibility is that a lack of solvent in
49
50
51
52
53
54
55
56
57
58
59
60

1
2
3 the ligand coating - perhaps coupled to residual surface stress associated with spin coating -
4
5 causes individual SiNCs to be 'darker' under these particular circumstances. In the presence of
6
7 other nanocrystals, however, it does not appear to be an issue, due presumably to the fast filling
8
9 of these trap states *via* energy transfer and subsequent relaxation mechanisms. Our results
10
11 suggest that this effect could make a substantial contribution to the PL stability of close-packed
12
13 nanocrystal solids, which will have important implications for any application that seeks to
14
15 exploit the PL from dense SiNC arrays. The trends reported here also likely represent a
16
17 foundation for a more precise explanation of the ensemble brightening reported for much larger
18
19 'bulk' SiNC structures,²¹ and quantitatively bridging these two effects will be the objective of
20
21 future work.
22
23
24
25
26
27

28 **Materials and Methods**

29
30 Plasma-synthesized SiNCs of nominal mean diameter 4 nm were passivated with 1-dodecene
31
32 as capping ligand to impart solubility in organic solvents⁸⁻¹¹ and separated by size using density-
33
34 gradient ultracentrifugation in chloroform/m-xylene mixtures, as detailed in the Supporting
35
36 Information.²¹⁻²³ Optical measurements were taken under a purified nitrogen atmosphere on a
37
38 customized inverted microscope using a 473 nm CW laser for excitation and a 60× 1.35 NA oil-
39
40 immersion objective for imaging. Dilute SiNC solutions were spin-coated on ultra-clean quartz
41
42 slides and the PL intermittency and background were measured immediately. After initiating
43
44 excitation, fast transients (comparable to the integration time) were allowed to relax prior to data
45
46 collection. A schematic of the experiment (Fig. S1) and additional details can be found in the
47
48 Supporting Information, along with typical movies of blinking ensembles.
49
50
51
52
53

54 Bright-field images were collected in order to identify large reference aggregates and a
55
56 digital grid was constructed based on these landmarks. Using this grid, specific PL signals were
57
58
59
60

1
2
3 then mapped onto SiNC clusters of varied size N via high-resolution atomic-force microscopy
4
5 (AFM) immediately after optical interrogation. The size of a reference cluster was corrected for
6
7 spatial resolution and packing effects to get cluster size N . Once the blinking behavior for a large
8
9 number of references had been directly correlated with the independently determined
10
11 agglomerate size for each sample and excitation power, a linear proportionality relation was
12
13 established between N and the average PL intensity (Fig. S2, Supporting Information) and these
14
15 linear relationships were then used to deduce N from the purely optical signals of many
16
17 thousands of assemblies for each scenario. Details can be found in the Supporting Information.
18
19
20

21
22 For DFT, we modeled the SiNCs as clusters of Si atoms in a bulk diamond structure, where
23
24 computational constraints require that the nanocrystals are smaller than those in the experiments.
25
26 For surface passivation, 2 or 1 methane groups were covalently bonded to each 2- or 3-
27
28 coordinated Si, respectively, to mimic experimental SiNC passivation by short alkyl chains. All
29
30 structures were optimized at the DFT level using the PBE1 hybrid functional and 6-31g* basis
31
32 set. Linear-response TD-DFT calculations, with the same functional and basis set, were
33
34 performed for all of the optimized structures to simulate the absorption spectra, where the first
35
36 100 excited states were calculated and a Gaussian line width of 0.08 eV was used to reproduce
37
38 inhomogeneous broadening of absorption spectra. Förster resonant energy transfer (FRET) rates
39
40 were then calculated between different SiNC donor/acceptor pairs based on the transition density
41
42 matrix, which goes beyond dipole-dipole coupling to include all multipole contributions. Details
43
44 can be found in the Supporting Information. Monte Carlo simulations for aggregates of non-
45
46 interacting SiNCs were obtained by first generating *on-off* trajectories for individual SiNCs
47
48 through an approach outlined in the Supporting Information. The simulation was specifically
49
50 designed to mimic the measurements. Blinking traces for assemblies composed of N non-
51
52
53
54
55
56
57
58
59
60

1
2
3 interacting SiNCs were then generated by adding N independent single SiNC spectra and
4
5 rebinning to 0 and 1. Details are given in the Supporting Information.
6
7
8
9

10 **ACKNOWLEDGMENTS**

11
12
13 The authors thank Dmitri Kilin and Boris Shklovskii for fruitful discussions and comments.
14
15 EKH acknowledges the support of the National Science Foundation (NSF) through CBET-
16 1133135 and US Department of Energy (DOE) through DE-FG36-08GO88160. RJA and URK
17
18 acknowledge primary support through the NSF under MRSEC grant DMR-0819885 and DMR-
19 1420013. KAV was supported by the Center for Advanced Solar Photophysics, an Energy
20
21 Frontier Research Center funded by the Office of Basic Energy Sciences, Office of Science,
22
23 DOE. SK acknowledges financial support of the DOE Early Career Research grant DE-
24
25 SC008446. For computational resources and administrative support, we thank the Center for
26
27 Computationally Assisted Science and Technology (CCAST) at North Dakota State University
28
29 and the National Energy Research Scientific Computing Center (NERSC) allocation award
30
31 86678, supported by the Office of Science of the DOE under contract No. DE-AC02-
32
33 05CH11231. Computational work was performed, in part, at the Center for Integrated
34
35 Nanotechnologies (CINT), an Office of Science User Facility operated for the DOE Office of
36
37 Science by Los Alamos National Laboratory (Contract DE-AC52-06NA25396) and Sandia
38
39 National Laboratories (Contract DE-AC04-94AL85000).
40
41
42
43
44
45
46
47

48 * erik.hobbie@ndsu.edu

49
50 § Present address – Rice University, Houston TX 77005

51
52 ¶ Present address – Michigan State University, East Lansing, MI 48824
53
54
55
56
57
58
59
60

1
2
3 **Supporting Information:** Details related to SiNC purification, experimental setup, cluster size
4 determination, blinking statistics, Monte Carlo simulations, and DFT calculations can be found
5
6 in the Supporting Information. This material is available free of charge *via* the Internet at
7
8 <http://pubs.acs.org>.
9
10

11 12 13 14 15 **References**

- 16
17 1. Howes, P. D.; Chandrawati, R.; Stevens, M. M. Colloidal Nanoparticles as Advanced
18 Biological Sensors. *Science* **2014**, *346*, 1247390.
19
20
- 21
22 2. Rakovich, T. Y.; Mahfoud, O. K.; Mohamed, B. M.; Prina-Mello, A.; Crosbie-Staunton, K.;
23 Van den Broeck, T.; De Kimpe, L.; Sukhanova, A.; Baty, D.; Rakovich, A.; *et al.* Highly
24 Sensitive Single Domain Antibody-Quantum Dot Conjugates for Detection of HER2 Biomarker
25 in Lung and Breast Cancer Cells. *ACS Nano* **2014**, *8*, 5682-5695.
26
27
- 28
29 3. Bruchez, M.; Moronne, M.; Gin, P.; Weiss, S.; Alivisatos, A. P. Semiconductor Nanocrystals
30 as Fluorescent Biological Labels. *Science* **1998**, *281*, 2013-2016.
31
32
- 33
34 4. Winnik, F. M.; Maysinger, D. Quantum Dot Cytotoxicity and Ways to Reduce It. *Acc. Chem.*
35 *Res.* **2012**, *46*, 672-680.
36
37
- 38
39 5. Contreras, E. Q.; Cho, M.; Zhu, H.; Puppala, H. L.; Escalera, G.; Zhong, W.; Colvin, V. L.
40 Toxicity of Quantum Dots and Cadmium Salt to *Caenorhabditis Elegans* after Multigenerational
41 Exposure. *Environ. Sci. Technol.* **2012**, *47*, 1148-1154.
42
43
- 44
45 6. Qu, Y.; Li, W.; Zhou, Y.; Liu, X.; Zhang, L.; Wang, L.; Li, Y.-F.; Iida, A.; Tang, Z.; Zhao, Y.;
46 *et al.* Full Assessment of Fate and Physiological Behavior of Quantum Dots Utilizing
47 *Caenorhabditis Elegans* as a Model Organism. *Nano Lett.* **2011**, *11*, 3174-3183.
48
49
50
51
52
53
54
55
56
57
58
59
60

- 1
2
3
4
5
6
7
8
9
10
11
12
13
14
15
16
17
18
19
20
21
22
23
24
25
26
27
28
29
30
31
32
33
34
35
36
37
38
39
40
41
42
43
44
45
46
47
48
49
50
51
52
53
54
55
56
57
58
59
60
7. Mangolini, L. Synthesis, Properties, and Applications of Silicon Nanocrystals. *J. Vac. Sci. & Tech. B* **2013**, *31*, 020801.
8. Anthony, R. J.; Rowe, D. J.; Stein, M.; Yang, J.; Kortshagen, U. Routes to Achieving High Quantum Yield Luminescence from Gas-Phase-Produced Silicon Nanocrystals. *Adv. Funct. Mater.* **2011**, *21*, 4042-4046.
9. Pi, X. D.; Liptak, R. W.; Nowak, J. D.; Wells, N.; Carter, C. B.; Campbell, S.; Kortshagen, U. Air-Stable Full-Visible-Spectrum Emission from Silicon Nanocrystal Ensembles Synthesized by an All-Gas-Phase Plasma Approach. *Nanotechnology* **2008**, *19*, 245603.
10. Mangolini, L.; Kortshagen, U. Plasma-Assisted Synthesis of Silicon Nanocrystal Inks. *Adv. Mater.* **2007**, *19*, 2513-2519.
11. Jurbergs, D.; Rogojina, E.; Mangolini, L.; Kortshagen, U. Silicon Nanocrystals with Ensemble Quantum Yields Exceeding 60 %. *Appl. Phys. Lett.* **2006**, *88*, 233116.
12. Hessel, C. M.; Reid, D.; Panthani, M. G.; Rasch, M. R.; Goodfellow, B. W.; Wei, J.; Fujii, H.; Akhavan, V.; Korgel, B. A. Synthesis of Ligand-Stabilized Silicon Nanocrystals with Size-Dependent Photoluminescence Spanning Visible to Near-Infrared Wavelengths. *Chem. Mat.* **2012**, *23*, 393-401.
13. Liu, S. M.; Yang, Y.; Sato, S.; Kimura, K. Enhanced Photoluminescence from Si Nano-Organosols by Functionalization with Alkenes and Their Size Evolution. *Chem. Mat.* **2006**, *18*, 637-642.
14. Zou, J.; Sanelle, P.; Pettigrew, K. A.; Kauzlarich, S. M., Size and Spectroscopy of Silicon Nanoparticles Prepared *via* Reduction of SiC₁₄. *J. Cluster Sci.* **2006**, *17*, 565-578.
15. Belomoin, G.; Therrien, J.; Nayfeh, M. Oxide and Hydrogen Capped Ultrasmall Blue Luminescent Si Nanoparticles. *Appl. Phys. Lett.* **2000**, *77*, 779-782.

- 1
2
3
4
5 16. Henderson, E. J.; Kelly, J. A.; Veinot, J. G. C. Influence of HSiO_{1.5} Sol-Gel Polymer
6 Structure and Composition on the Size and Luminescent Properties of Silicon Nanocrystals.
7 *Chem. Mater.* **2009**, *21*, 5426-5434.
8
9
10
11
12 17. Mastronardi, M. L.; Maier-Flaig, F.; Faulkner, D.; Henderson, E. J.; Kübel, C.; Lemmer, U.;
13 Ozin, G. A. Size-Dependent Absolute Quantum Yields for Size-Separated Colloidally-Stable
14 Silicon Nanocrystals. *Nano Lett.* **2012**, *12*, 337-342.
15
16
17
18
19 18. Locritani, M; Yu, Y.; Bergamini, G.; Baroncini, M.; Molloy, J. K.; Korgel, B. A.; Ceroni, P.
20 Silicon Nanocrystals Functionalized with Pyrene Units: Efficient Light-Harvesting Antennae
21 with Bright Near-Infrared Emission. *J. Phys. Chem. Lett.* **2014**, *5*, 3325-3329.
22
23
24
25
26 19. Sugimoto, H.; Fujii, M.; Imakita, K. Synthesis of Boron and Phosphorus Codoped All-
27 Inorganic Colloidal Silicon Nanocrystals from Hydrogen Silsesquioxane. *Nanoscale* **2014**, *6*,
28 12354-12359.
29
30
31
32
33 20. Sugimoto, H.; Fujii, M.; Fukuda, Y.; Imakita, K.; Akamatsu, K. All-Inorganic Water-
34 Dispersible Silicon Quantum Dots: Highly Efficient Near-Infrared Luminescence in a Wide pH
35 Range. *Nanoscale* **2014**, *6*, 122-126.
36
37
38
39
40 21. Miller, J. B.; Van Sickle, A. R.; Anthony, R. J.; Kroll, D. M.; Kortshagen, U. R.; Hobbie, E.
41 K. Ensemble Brightening and Enhanced Quantum yield in Size-Purified Silicon Nanocrystals,
42 *ACS Nano* **2012**, *6*, 7389-7396.
43
44
45
46
47 22. Miller, J. B.; Harris, J. M.; Hobbie, E. K. Purifying Colloidal Nanoparticles through
48 Ultracentrifugation with Implications for Interfaces and Materials. *Langmuir* **2014**, *30*, 7936-
49 7946.
50
51
52
53
54 23. Miller, J. B.; Hobbie, E. K. Nanoparticles as Macromolecules. *J. Polym. Sci. B - Polym.*
55 *Phys.* **2013**, *51*, 1195-1208.
56
57
58
59
60

- 1
2
3
4
5 24. Mastronardi, M. L.; Hennrich, F.; Henderson, E. J.; Maier-Flaig, F.; Blum, C.; Reichenbach,
6 J.; Lemmer, U.; Kübel, C.; Wang, D.; Kappes, M. M.; *et al.* Preparation of Monodisperse Silicon
7 Nanocrystals Using Density Gradient Ultracentrifugation. *J. Am. Chem. Soc.* **2011**, 133, 11928-
8 11931.
- 9
10
11
12
13
14 25. Erogbogbo, F.; Yong, K.-T.; Roy, I.; Xu, G.; Prasad, P. N.; Swihart, M. T. Biocompatible
15 Luminescent Silicon Quantum Dots for Imaging of Cancer Cells. *ACS Nano* **2008**, 2, 873-878.
- 16
17
18
19 26. Fujioka, K.; Hiruoka, M.; Sato, K.; Manabe, N.; Miyasaka, R.; Hanada, S.; Hoshino, A.;
20 Tilley, R. D.; Manome, Y.; Hirakuri, K.; *et al.* Luminescent Passive-Oxidized Silicon Quantum
21 Dots as Biological Staining Labels and Their Cytotoxicity Effects at High Concentration.
22 *Nanotechnology* **2008**, 19, 415102.
- 23
24
25
26
27
28 27. McVey, B. F. P.; Tilley, R. D. Solution Synthesis, Optical Properties and Bioimaging
29 Applications of Silicon Nanocrystals. *Accts. Chem. Res.* **2014**, 47, 3045-3051.
- 30
31
32
33 28. Sychugov, I.; Fucikova, A.; Pevere, F.; Yang, Z.; Veinot, J. G. C.; Linnros, J. Ultranarrow
34 Luminescence Linewidth of Silicon Nanocrystals and Influence of Matrix. *ACS Photonics* **2014**,
35 1, 998-1005.
- 36
37
38
39
40 29. Yang, Z.; Dasog, M.; Dobbie, A. R.; Lockwood, R.; Zhi, Y.; Meldrum, A.; Veinot, J. G. C.
41 Highly Luminescent Covalently Linked Silicon Nanocrystal/Polystyrene Hybrid 26. Functional
42 Materials: Synthesis, Properties, and Processability. *Adv. Funct. Mater.* **2014**, 24, 1345-1353.
- 43
44
45
46
47 30. Van Sickle, A. R.; Miller, J. B.; Moore, C.; Anthony, R. J.; Kortshagen, U. R.; Hobbie, E. K.
48 Temperature Dependent Photoluminescence of Size-Purified Silicon Nanocrystals. *ACS Appl.*
49 *Mater. & Interfaces* **2013**, 5, 4233-4238.
- 50
51
52
53
54 31. Dohnalova, K.; Gregorkiewicz, T.; Kusova, K. Silicon Quantum Dots: Surface Matters. *J.*
55 *Phys.-Cond. Matt.* **2014**, 26, 173201.
- 56
57
58
59
60

- 1
2
3
4
5 32. Dohnalová, K.; Poddubny, A. N.; Prokofiev, A. A.; de Boer, W. D. A. M.; Umesh, C. P.;
6 Paulusse, J. M. J.; Zuilhof, H.; Gregorkiewicz, T. Surface Brightens up Si Quantum Dots: Direct
7 Bandgap-Like Size-Tunable Emission. *Light: Sci. Appl.* **2013**, *2*, e47.
8
9
10
11
12 33. Kallel, H.; Arbouet, A.; Carrada, M.; Ben Assayag, G.; Chehaidar, A.; Periwal, P.; Baron, T.;
13 Normand, P.; Paillard, V. Photoluminescence Enhancement of Silicon Nanocrystals Placed in the
14 Near Field of a Silicon Nanowire. *Phys. Rev. B* **2013**, *88*, 081302.
15
16
17
18
19 34. Valenta, J.; Greben, M.; Gutsch, S.; Hiller, D.; Zacharias, M. Effects of Inter-Nanocrystal
20 Distance on Luminescence Quantum Yield in Ensembles of Si Nanocrystals. *Appl. Phys. Lett.*
21 **2014**, *105*, 243107.
22
23
24
25
26 35. Tice, D. B.; Frederick, M. T.; Chang, R. P. H.; Weiss, E. A. Electron Migration Limits the
27 Rate of Photobrightening in Thin Films of CdSe Quantum Dots in a Dry N₂ (g) Atmosphere. *J.*
28 *Phys. Chem. C* **2011**, *115*, 3654-3662.
29
30
31
32
33 36. Hua, Z.; Xu, Q. F.; Huang, X. N.; Zhang, C. F.; Wang, X. Y.; Xiao, M. Energy Transfer from
34 a Single Semiconductor Nanocrystal to Dye Molecules. *ACS Nano* **2014**, *8*, 7060-7066.
35
36
37
38
39 37. Ajayi, O. A.; Anderson, N. C.; Cotlet, M.; Petrone, N.; Gu, T.; Wolcott, A.; Gesuele, F.;
40 Hone, J.; Owen, J. S.; Wong, C. W. Time-Resolved Energy Transfer from Single Chloride-
41 Terminated Nanocrystals to Graphene. *Appl. Phys. Lett.* **2014**, *104*, 171101.
42
43
44
45
46 38. Xu, Z.; Hine, C.; Maye, M.; Cotlet, M. Shell-Thickness Dependent Hole Transfer in
47 Conjugated Polymer/Quantum Dot Hybrids, *ACS Nano* **2012**, *6*, 4984-4992.
48
49
50
51 39. Nguyen, H. M.; Seitz, O.; Peng, W. N.; Gartstein, Y. N.; Chabal, Y. J.; Malko, A. V.
52 Efficient Radiative and Nonradiative Energy Transfer from Proximal CdSe/ZnS Nanocrystals
53 into Silicon Nanomembranes. *ACS Nano* **2012**, *6*, 5574-5582.
54
55
56
57
58
59
60

- 1
2
3
4
5
6
7
8
9
10
11
12
13
14
15
16
17
18
19
20
21
22
23
24
25
26
27
28
29
30
31
32
33
34
35
36
37
38
39
40
41
42
43
44
45
46
47
48
49
50
51
52
53
54
55
56
57
58
59
60
40. Fernee, M. J.; Tamarat, P.; Lounis, B. Spectroscopy of Single Nanocrystals. *Chem. Soc. Rev.* **2014**, *43*, 1311-1337.
41. Vanmaekelbergh, D.; Casavola, M. Single-Dot Microscopy and Spectroscopy for Comprehensive Study of Colloidal Nanocrystals. *J. Phys. Chem. Lett.* **2011**, *2*, 2024-2031.
42. Galland, C.; Ghosh, Y.; Steinbruck, A.; Sykora, M.; Hollingsworth, J. A.; Klimov, V. I.; Htoon, H. Two Types of Luminescence Blinking Revealed by Spectroelectrochemistry of Single Quantum Dots. *Nature* **2011**, *479*, 203-207.
43. Pelton, M.; Smith, G.; Scherer, N. F.; Marcus, R. A. Evidence for a Diffusion-Controlled Mechanism for Fluorescence Blinking of Colloidal Quantum Dots. *PNAS* **2007**, *104*, 14249-14254.
44. Tang, J.; Marcus, R. A. Determination of Energetics and Kinetics from Single-Particle Intermittency and Ensemble-Averaged Fluorescence Intensity Decay of Quantum Dots. *J. Chem. Phys.* **2006**, *125*, 044703.
45. Durisic, N.; Wiseman, P. W.; Gruetter, P.; Heyes, C. D. A Common Mechanism Underlies the Dark Fraction Formation and Fluorescence Blinking of Quantum Dots. *ACS Nano* **2009**, *3*, 1167-1175.
46. Cichos, F.; von Borczyskowski, C.; Orrit, M. Power-Law Intermittency of Single Emitters. *Curr. Opin. Colloid Interface Sci.* **2007**, *12*, 272-284.
47. Schmidt, R.; Krasselt, C.; Goehler, C.; von Borczyskowski, C. The Fluorescence Intermittency for Quantum Dots Is Not Power-Law Distributed: A Luminescence Intensity Resolved Approach. *ACS Nano* **2014**, *8*, 3506-3521.
48. Bruhn, B.; Qejvanaj, F.; Gregorkiewicz, T.; Linnros, J. Temporal Correlation of Blinking Events in CdSe/ZnS and Si/SiO₂ Nanocrystals. *Phys. B - Cond. Matt.* **2014**, *453*, 63-67.

- 1
2
3
4
5 49. Hefti, R.; Jones, M.; Moyer, P. J. Long-Range Correlated Fluorescence Blinking in
6 CdSe/ZnS Quantum Dots. *J. Phys. Chem. C* **2012**, *116*, 25617-25622.
7
8
9
10 50. Osborne, M. A.; Lees, S. F. Quantum Dot Photoluminescence Activation and Decay: Dark,
11 Bright, and Reversible Populations in ZnS-Capped CdSe Nanocrystals. *ACS Nano* **2011**, *5*, 8295-
12 8304.
13
14
15
16
17 51. Volkan-Kacso, S.; Frantsuzov, P. A.; Janko, B. Correlations between Subsequent Blinking
18 Events in Single Quantum Dots. *Nano Lett.* **2010**, *10*, 2761-2765.
19
20
21
22
23 52. Goushi, K.; Yamada, T.; Otomo, A. Excitation Intensity Dependence of Power-Law Blinking
24 Statistics in Nanocrystal Quantum Dots. *J. Phys. Chem. C* **2009**, *113*, 20161-20168.
25
26
27
28 53. Chung, I.; Witkoskie, J. B.; Cao, J. S.; Bawendi, M. G. Description of the Fluorescence
29 Intensity Time Trace of Collections of CdSe Nanocrystal Quantum Dots based on Single
30 Quantum Dot Fluorescence Blinking Statistics. *Phys. Rev. E* **2006**, *73*, 011106.
31
32
33
34
35 54. Tang, J.; Marcus, R. A. Mechanisms of Fluorescence Blinking in Semiconductor Nanocrystal
36 Quantum Dots. *J. Chem. Phys.* **2005**, *123*, 054704.
37
38
39
40 55. Verberk, R.; Orrit, M. Photon Statistics in the Fluorescence of Single Molecules and
41 Nanocrystals: Correlation Functions *versus* Distributions of On- and Off-Times. *J. Chem. Phys.*
42 **2003**, *119*, 2214-2222.
43
44
45
46
47 56. Crouch, C. H.; Sauter, O.; Wu, X.; Purcell, R.; Querner, C.; Drndic, M.; Pelton, M.; Facts and
48 Artifacts in the Blinking Statistics of Semiconductor Nanocrystals. *Nano Lett.* **2010**, *10*, 1692-
49 1698.
50
51
52
53
54 57. Amecke, A.; Heber, A.; Cichos, F. Distortion of Power Law Blinking with Binning and
55 Thresholding. *J. Chem. Phys.* **2014**, *140*, 114306.
56
57
58
59
60

- 1
2
3
4
5 58. Houel, J.; Doan, Q. T.; Cajgfinger, T.; Ledoux, G.; Amans, D.; Aubret, A.; Dominjon, A.;
6 Ferriol, S.; Barbier, R.; Nasilowski, M.; *et al.* Autocorrelation Analysis for the Unbiased
7 Determination of Power-Law Exponents in Single-Quantum-Dot Blinking. *ACS Nano* **2015**, *9*,
8 886-893.
9
10
11
12
13
14 59. English, D. S.; Pell, L. E.; Yu, Z.; Barbara, P. F.; Korgel, B. A. Size Tunable Visible
15 Luminescence from Individual Organic Monolayer Stabilized Silicon Nanocrystal Quantum
16 Dots. *Nano Lett.* **2002**, *2*, 681-685.
17
18
19
20
21 60. Munro, A. M.; Ginger, D. S. Photoluminescence Quenching of Single CdSe Nanocrystals by
22 Ligand Adsorption. *Nano Lett.* **2008**, *8*, 2585-2590.
23
24
25
26 61. Chizhik, A. I.; Schmidt, T.; Chizhik, A. M.; Huisken, F.; Meixner, A. J. Dynamical Effects of
27 Defect Photoluminescence from Single SiO₂ and Si Nanoparticles. *Phys. Procedia* **2011**, *13*, 28-
28 32.
29
30
31
32
33 62. Califano, M.; Gomez-Campos, F. M. Universal Trapping Mechanism in Semiconductor
34 Nanocrystals. *Nano Lett.* **2013**, *13*, 2047-2052.
35
36
37
38
39 63. Mangum, B. D.; Wang, F.; Dennis, A. M.; Gao, Y. Q.; Ma, X. D.; Hollingsworth, J. A.;
40 Htoon, H. Competition between Auger Recombination and Hot-Carrier Trapping in PL Intensity
41 Fluctuations of Type II Nanocrystals. *Small* **2014**, *10*, 2892-2901.
42
43
44
45
46 64. Bell, D. M.; Howder, C. R.; Johnson, R. C.; Anderson, S. L. Single CdSe/ZnS Nanocrystals
47 in an Ion Trap: Charge and Mass Determination and Photophysics Evolution with Changing
48 Mass, Charge, and Temperature. *ACS Nano* **2014**, *8*, 2387-2398.
49
50
51
52
53 65. Tenne, R.; Teitelboim, A.; Rukenstein, P.; Dyshel, M.; Mokari, T.; Oron, D. Studying
54 Quantum Dot Blinking through the Addition of an Engineered Inorganic Hole Trap. *ACS Nano*
55 **2013**, *7*, 5084-5090.
56
57
58
59
60

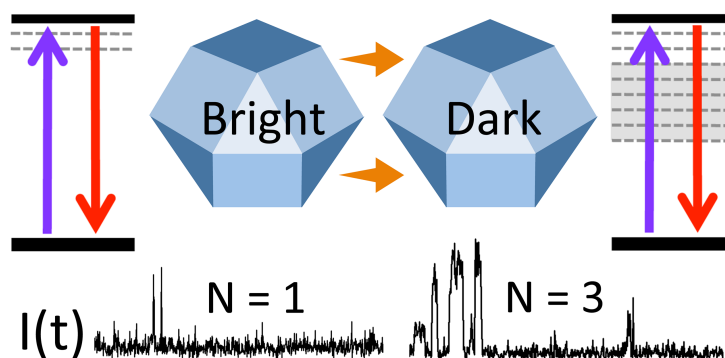
- 1
2
3
4
5 66. Li, S.; Steigerwald, M. L.; Brus, L. E. Surface States in the Photoionization of High-Quality
6 CdSe Core/Shell Nanocrystals. *ACS Nano* **2009**, *3*, 1267-1273.
7
8
9
10 67. Wang, X. Y.; Ren, X. F.; Kahen, K.; Hahn, M. A.; Rajeswaran, M.; Maccagnano-Zacher, S.;
11 Silcox, J.; Cragg, G. E.; Efros, A. L.; Krauss, T. D. Non-Blinking Semiconductor Nanocrystals.
12 *Nature* **2009**, *459*, 686-689.
13
14
15
16
17 68. Park, Y. S.; Bae, W. K.; Padilha, L. A.; Pietryga, J. M.; Klimov, V. I. Effect of the
18 Core/Shell Interface on Auger Recombination Evaluated by Single-Quantum-Dot Spectroscopy,
19 *Nano Lett.* **2014**, *14*, 396-402.
20
21
22
23
24 69. Zhang, A. D.; Dong, C. Q.; Liu, H.; Ren, J. C. Blinking Behavior of CdSe/CdS Quantum
25 Dots Controlled by Alkylthiols as Surface Trap Modifiers. *J. Phys. Chem. C* **2013**, *117*, 24592-
26 24600.
27
28
29
30
31 70. Early, K. T.; Nesbitt, D. J. Size-Dependent Photoionization in Single CdSe/ZnS
32 Nanocrystals. *Nano Lett.* **2013**, *13*, 4844-4849.
33
34
35
36
37 71. Qin, W.; Guyot-Sionnest, P. Evidence for the Role of Holes in Blinking: Negative and
38 Oxidized CdSe/CdS Dots. *ACS Nano* **2012**, *6*, 9125-9132.
39
40
41
42 72. Jin, S.; Song, N.; Lian, T. Suppressed Blinking Dynamics of Single QDs on ITO. *ACS Nano*
43 **2010**, *4*, 1545-1552.
44
45
46
47 73. Velizhanin, K. A.; Piryatinski, A.; Chernyak, V. Y. Low-Temperature Hopping Dynamics
48 with Energy Disorder: Renormalization Group Approach. *J. Chem. Phys.* **2013**, *139*, 084118.
49
50
51
52 74. Brawand, N. P.; Voros, M.; Galli, G. Surface Dangling Bonds are a Cause of B-Type
53 Blinking in Si Nanoparticles. *Nanoscale* **2015**, *7*, 3737-3744.
54
55
56
57
58
59
60

- 1
2
3
4
5
6
7
8
9
10
11
12
13
14
15
16
17
18
19
20
21
22
23
24
25
26
27
28
29
30
31
32
33
34
35
36
37
38
39
40
41
42
43
44
45
46
47
48
49
50
51
52
53
54
55
56
57
58
59
60
75. Lin, Z.; Li, H.; Franceschetti, A.; Lusk, M. T. Efficient Exciton Transport between Strongly Quantum-Confined Silicon Quantum Dots. *ACS Nano* **2012**, *6*, 4029-4038.
76. Allan, G.; Delerue, C. Energy Transfer between Semiconductor Nanocrystals: Validity of Förster's Theory. *Phys. Rev. B* **2007**, *75*, 195311.
77. Bruhn, B.; Valenta, J.; Sangghaleh, F.; Linnros, J. Blinking Statistics of Silicon Quantum Dots. *Nano Lett.* **2011**, *11*, 5574-5580.
78. Valenta, J.; Fucikova, A.; Vacha, F.; Adamec, F.; Humpolickova, J.; Hof, M.; Pelant, I.; Kusova, K.; Dohnalova, K.; Linnros, J. Light-Emission Performance of Silicon Nanocrystals Deduced from Single Quantum Dot Spectroscopy. *Adv. Funct. Mater.* **2008**, *18*, 2666-2672.
79. Cichos, F.; Martin, J.; von Borczyskowski, C. Emission Intermittency in Silicon Nanocrystals. *Phys. Rev. B* **2004**, *70*, 115314.
80. Wintle, H. J. Decay of Static Electrification by Conduction Processes in Polyethylene. *J. Appl. Phys.* **1970**, *41*, 4004-4007.
81. Whitcomb, K. J.; Ryan, D. P.; Gelfand, M. P.; Van Orden, A. Blinking Statistics of Small Clusters of Semiconductor Nanocrystals. *J. Phys. Chem. C* **2013**, *117*, 25761-25768.
82. Wang, S. Y.; Querner, C.; Dadosh, T.; Crouch, C. H.; Novikov, D. S.; Drndic, M. Collective Fluorescence Enhancement in Nanoparticle Clusters. *Nature Comm.* **2011**, 364.
83. Shepherd, D. P.; Whitcomb, K. J.; Milligan, K. K.; Goodwin, P. M.; Gelfand, M. P.; Van Orden, A. Fluorescence Intermittency and Energy Transfer in Small Clusters of Semiconductor Quantum Dots. *J. Phys. Chem. C* **2010**, *114*, 14831-14837.
84. Wang, S.; Querner, C.; Fischbein, M. D.; Willis, L.; Novikov, D. S.; Crouch, C. H.; Drndic, M. Blinking Statistics Correlated with Nanoparticle Number. *Nano Lett.* **2008**, *8*, 420-426.

1
2
3
4
5 85. Yu, M.; Van Orden, M. Enhanced Fluorescence Intermittency of CdSe-ZnS Quantum-Dot
6 Clusters. *Phys. Rev. Lett.* **2006**, *97*, 237402.
7
8

9
10 86. Kowerko, D.; Schuster, J.; Amecke, N.; Abdel-Mottaleb, M.; Dobrawa, R.; Wurthner, F.; von
11 Borczyskowski, C. FRET and Ligand Related Non-FRET Processes in Single Quantum Dot-
12 Perylene Bisimide Assemblies. *Phys. Chem. Chem. Phys.* **2010**, *12*, 4112-4123.
13
14

15
16 87. Akselrod, G. M.; Prins, F.; Poulidakos, L. V.; Lee, E. M.; Weidman, M. C.; Mork, A. J.;
17 Willard, A. P.; Bulović, V.; Tisdale, W. A. Subdiffusive Exciton Transport in Quantum Dot
18 Solids. *Nano Lett.* **2014**, *14*, 3556-3562.
19
20
21
22



TOC Graphic